Jo rnal of ELECTRONIC MATERIALS, Vol. 45, No. 4, 2016
DOI: 10.1007/s11664-016-4387-7

O a f a C B ffe- P a f - f - M c l eg-a f l GaN/GaN L g -E g D de a d A GaN/GaN H g -E ec - -M b T-a -

CHAO LIU,[1] YUEFEI CAI,[1] HUAXING JIANG,[1] and KEI MAY LAU[1,2]

1. Photonics Technolog Center, Department of Electronic and Comp ter Engineering, Hong Kong Uni ersit of Science and Technolog , Clear Water Ba , Ko loon, Hong Kong. 2. e-mail: eekmla @ st.hk

For the de elopment of a metal-interconnection-free integration scheme for monolithic integration of InGaN/GaN light-emitting diodes (LEDs) and AlGaN/GaN high-electron-mobilit transistors (HEMTs), a common b ffer to achie e high brightness, lo leakage c rrent, and high breakdo n in the integrated HEMT LED de ice is essential. Different b ffer str ct res ha e been in esti-gated, and their impacts pon both the LED and HEMT parts of the HEMT LED de ice ha e been anal ed. Res lts indicated that a GaN/AlN b ffer str ct re is the most ideal to ser e as a common b ffer platform, offering both the e cellent cr stalline q alit and s perior b ffer resisti it req ired b the HEMT LED de ice. Gro th of the AlN la er as partic larl cr cial for engi-neering the dislocation densit , s rface morpholog , as ell as resisti it of the b ffer la er. Using the optimi ed GaN/AlN b ffer str ct re, the LED part of the HEMT LED de ice as impro ed, sho ing greatl enhanced light o tp t po er and s ppressed re erse leakage c rrent, hile the breakdo n charac-teristics of the HEMT part ere also impro ed.

Key words: Metalorganic chemical apor deposition, light-emitting diodes, high-electron-mobilit transistors, HEMT LED integration

INTRODUCTION

Integration of InGaN/GaN light-emitting diodes (LEDs) and AlGaN/GaN high-electron-mobilit transistors (HEMTs) on a common material platform is attracting interest d e to its ad antages in red cing de ice footprint, enhancing s stem reliabilit , and minimi ing interconnect-related parasitics.[1] To accomplish a monolithicall integrated HEMT LED de ice, a fe different schemes ha e been reported, incl ding selecti e epi remo al (SER), selecti e epita ial gro th (SEG), and afer bonding techniq es.[2–8] Recentl , e demonstrated a metal-interconnection-free scheme for HEMT LED inte-gration b combining SER and SEG proced res. A schematic of the monolithicall integrated HEMT LED str ct re is sho n in Fig. 1. Ke to this method is obtaining intimate and seamless contact bet een the GaN channel of the HEMT and the *n*-t pe la er of the LED. Effecti e mod lation of the LED brightness b gate control of the dri ing c rrent injected thro gh the HEMT has been demonstrated.[9] Ho e er, d e to the difference in material req irements for the LED and HEMT, it is not tri ial to achie e high brightness in the LED part and high breakdo n in the HEMT part sim ltaneo sl . A common b ffer platform ith both high cr stalline q alit and high resisti it for the monolithicall integrated HEMT LED de ice that can lead to this goal is therefore highl desirable.

In earl st dies, a t o-step gro th proced re sing lo -temperat re GaN (LT-GaN) as n cleation la er as t picall sed to promote t o-dimensional (2D) GaN gro th on sapphire.[10] After ards, se eral gro ps demonstrated that an intentionall prolonged three-dimensional (3D) gro th mode in the earl stage of GaN gro th co ld effecti el red ce the

(Recei ed A g st 20, 2015; accepted Febr ar 3, 2016; p blished online Febr ar 18, 2016)

threading dislocation densit and impro e the cr stalline q alit ,[11,12] boosting the performance of GaN-based light-emitting diodes. Ho e er, it as recentl fo nd that the 3D gro th mode as accompanied b enhanced nintentional doping that introd ces a b ried cond cti e channel and degrades the b ffer breakdo n;[13,14] being the most ndesirable characteristics for transistors. Altho gh acceptor-like imp rities (e.g., Fe, Mg) can be introd ced to compensate the backgro nd donor states and enhance the resisti it of the GaN b ffer la er,[15–18] Mg and Fe are kno n to ha e serio s memor effects,[16,17] potentiall redistrib ting to ards the channel region and degrading de ice performance. A high-resisti it b ffer itho t compensating dopants that also eliminates the cond cti e channel ind ced b the 3D gro th mode[19] o ld be most ideal. The alternati e of GaN b ffers on sapphire sing AlN as n cleation la er o ld not introd ce leak channels and co ld potentiall pro ide high cr stalline q alit and high b ffer resisti it sim ltaneo sl .[20–24] Ho e er, gro th of this kind of GaN b ffers occ rs in a narro gro th indo . The best cr stalline q alit and s rface morpholog can onl be achie ed hen neither Al nor N atoms dominate at the s rface.[25,26]

To optimi e the integrated HEMT LED performance, e ha e de eloped a GaN/AlN b ffer platform feat ring high b ffer resisti it and e cellent cr stalline q alit sim ltaneo sl . The infl ence of the gro th temperat re and the V/III ratio of the AlN la er on the cr stalline q alit and s rface morpholog of the pper AlGaN/GaN heterostr ct res has been in estigated. Under optimal AlN gro th conditions, the dislocation densit in the GaN b ffer can be red ced to 3.2×10^8 cm^{-2} ith high resisti it . To erif the ad antages of the GaN/AlN b ffer str ct re, e st died the effect of different b ffer str ct res on the performance of the HEMT and LED parts of the HEMT LED de ice. Based on the high-q alit GaN/AlN b ffer, impro ed light o tp t po er and s ppressed re erse leakage c rrent ere achie ed in the LED part. Mean hile, lo b ffer leakage as achie ed. Therefore, the GaN/AlN b ffer str ct re de eloped in this ork is promising to ser e as a common platform for HEMT LED integration.

EXPERIMENTAL PROCEDURES

This st d as carried o t sing a pre io sl pro en scheme for the integrated de ice.[9] The AlGaN/GaN HEMT str ct res sed in this ork ere gro n on 2-inch sapphire s bstrates in an Ai tron 2400HT metalorganic chemical apor deposition (MOCVD) s stem. Trimeth lgalli m (TMGa), trimeth lal min m (TMAl), and ammonia (NH_3) ere sed as Ga, Al, and N so rce, respecti el . Nitrogen and h drogen ere sed as carrier gas. Three b ffer str ct res ere sed for AlGaN/GaN HEMT gro th In this ork, as sho n in Fig. 2. With different temperat re ramping rates and parameters for the initial high-temperat re GaN gro th, high-q alit (HQ) and high-resisti it (HR) GaN b ffers on sapphire can be achie ed, respecti el , as sho n in Fig. 2a and b. The HQ GaN b ffer as gro n sing the method idel adopted for gro ing LEDs on sapphire. A 25-nm GaN n cleation la er as deposited at 550°C, follo ed b temperat re ramping to 1150°C in 7 min and *in situ* annealing for 2 min. D ring the annealing, small grains start to decompose, lea ing a lo densit of large grains. This as follo ed b high-temperat re GaN b ffer gro th at 200 mbar. Three-dimensional (3D) grain gro th first occ rs on the island-like grains of the n cleation la er prior to the t o-dimensional (2D) coalesced gro th. The 3D-to-2D transition gro th mode as accompanied ith epita ial lateral o ergro th (ELOG), hich can effecti el red ce the threading dislocation densit . Mean hile, for HR GaN b ffer gro th, the reactor temperat re as ramped p to 1050°C in 3 min after lo -temperat re GaN n cleation, follo ed b immediate gro th of high-temperat re GaN at 50 mbar. The increased temperat re ramping rate itho t annealing helped to maintain a q asi-2D morpholog for the lo -temperat re GaN n cleation la er. Moreo er, the lo er reactor press re can ens re direct 2D gro th for the high-temperat re GaN. As a res lt, nintentional doping d ring the 3D gro th can be a oided and the leakage channel at the sapphire GaN interface eliminated.

Alternati el , AlGaN/GaN HEMTs sing GaN/AlN b ffer ere also in estigated, as sho n in Fig. 2c. To optimi e the GaN/AlN b ffer for HEMT applications, a series of gro th e periments ere carried o t. With the thickness of the AlN n cleation la er kept at 150 nm, the gro th conditions of the AlN la er for fi e samples ere aried as listed in Table I. The reactor press re as fi ed a00037(p3

the V/III ratio during AlN growth. Atomic force microscopy (AFM) and high-resolution x-ray diffraction (HRXRD) were used to characterize the surface morphology and crystalline quality of the as-grown AlGaN/GaN HEMT epi on top. Mercury capacitance–voltage (*C*–*V*) probe measurements were implemented to determine the background carrier concentration and monitor the leakage channel in the buffer layer. The electron transport properties of the AlGaN/GaN HEMT epi were investigated by van der Pauw Hall measurements, using ohmic contacts formed by alloyed indium dots on the AlGaN barrier. Afterwards, the AlGaN/GaN stack was selectively removed by inductively coupled plasma (ICP) etching, exposing the GaN buffer underneath for subsequent LED overgrowth. The overgrown LED structure consisted of 1.5-μm *n*-type GaN, five periods of $In_{0.1}Ga_{0.9}N$/GaN multiquantum wells (MQWs) with 3-nm-thick wells and 12-nm-thick barriers, followed by a 15-nm *p*-type $Al_{0.15}Ga_{0.85}N$ and a 170-nm *p*-type GaN layer. After the growth, both discrete LEDs and integrated HEMT–LEDs were fabricated. Details of the fabrication process can be found in Ref. 9. Electrical properties were measured by on-wafer probing, and luminescence properties were collected using a calibrated integrating sphere at room temperature.

RESULTS AND DISCUSSION

Figure 3a, b, and c show the surface morphologies of the AlGaN/GaN HEMTs grown on GaN/AlN buffers with AlN deposited at 950°C, 1050°C, and 1150°C, respectively (labeled sample A, B, and C, respectively). Fragmented surface morphology with large and deep pits can be observed for sample A. This is due to incomplete coalescence of the initial 3D AlN islands at low temperature. When the AlN temperature was increased to 1050°C in sample B, step-flow morphology can be observed on the final AlGaN/GaN surface, with root-mean-square (RMS) roughness decreased from 4.5 nm to 0.8 nm. The associated large density of surface pits lowers the effective barrier height and increases the reverse gate leakage current of the fabricated HEMT devices.[27] When the AlN temperature was further increased to 1150°C, sample C showed a pit-free surface with RMS roughness of 0.3 nm, which can be attributed to the enhanced Al atom mobility at higher temperature.

In addition to the AlN growth temperature, the V/III ratio of the AlN layer also plays an important role in the surface morphologies of the upper AlGaN/GaN HEMTs. It is well known that inversion domains can form during AlN growth if there is prereaction between NH_3 and Al_2O_3, causing mixed domains and thus rough surface.
[illegible]

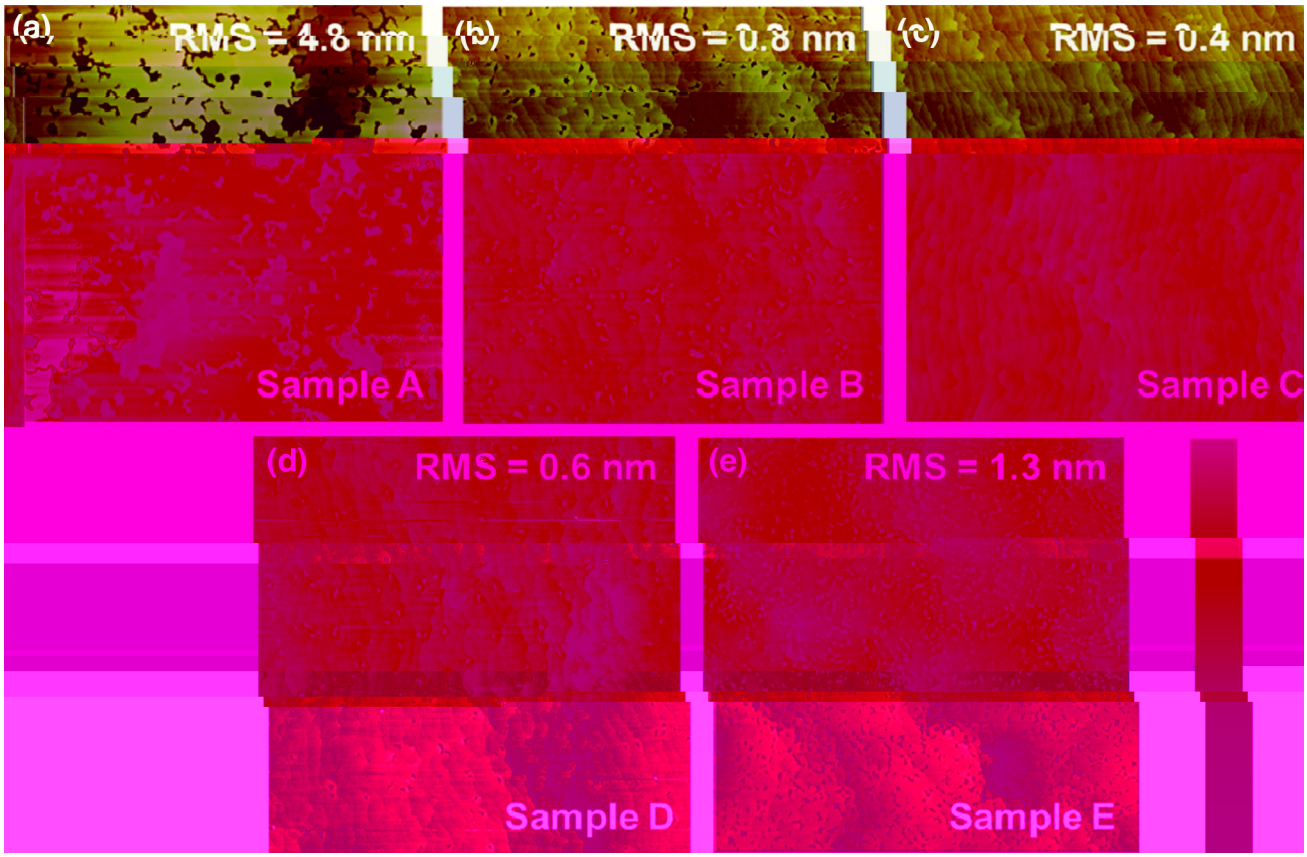

F g. 3. S face g f a e A E, d ffe e AN g c d . A ca a e 5 μ × 5 μ ; e ca ca e ba a e 15 , 5 , 5 , a d 10 f a e A E, e ec e (C fig e e).

preflo as sed, b t optimi ing the ammonia flo at high temperat re as fo nd to be effecti e. Fig re 3c e depicts the depe dence of the s rface morpholog on the V/III ratio of the AlN la er at fi ed gro th temperat re of 1150°C and reactor press re of 50 mbar. The lo est densit of s rface pits on the AlGaN/GaN HEMT s rface as obtained ith a V/III ratio of 550 (sample C). The pinholes ma be either attrib ted to in ersion domains or d e to threading dislocations that terminate at the sample s rface.[30]

The dependence of the cr stalline q alit and s rface ro ghness of the AlGaN/GaN/AlN heterostr ct res on the gro th temperat re and V/III ratio of the AlN la er is plotted in Fig. 4. The FWHM al e of the GaN/AlN b ffer decreased monotonicall ith increased AlN gro th tempera-t re, hereb enhanced Al atom mobilit can lead to red ced misorientations and n clei densit in the AlN la er. As a res lt, fe er threading dislocations can penetrate into the pper GaN b ffer, and impro ed cr stalline q alit can be ach e ed. This phenomenon agrees ith the res lts reported b Li et al.[31] The V/III ratio of the AlN la er gro th also affects the cr stalline q alit of the pper GaN b ffer, ith a minimal FWHM al e at V/III ratio of 500. F rthermore, it is orth noting that the s rface ro ghness and XRD line idth e hibited similar trends ith gro th temperat re. This coin-cidence indicates that, ith red ced misorientations and n clei densities of the initial AlN n clei nder the optimal AlN gro th condition, red ced s rface ro ghness and impro ed cr stalline q alit can be ach e ed sim ltaneo sl .

Using the optim m AlN gro th condition described abo e, an AlGaN/GaN HEMT str ct re as gro n sing the GaN/AlN b ffer str ct re, to be compared ith t o other HEMT samples gro n sing con entional HQ GaN b ffer and HR GaN b ffer, respecti el . The s rface morphologies of the as-gro n AlGaN/GaN HEMT epi on different b ffer str ct res ere compared b AFM (Fig. 5). Well-aligned step flo co ld be obser ed for the HEMT on the HQ GaN b ffer, ith an RMS al e of 0.4 nm. The RMS al e of the AlGaN/GaN s rface ith HR GaN b ffer increased to 0.6 nm, accompanied b disordered step flo , d e to increased misorienta-tions and n clei densit of the GaN n cleation la er b eliminating the 3D-to-2D transition gro th mode. The AlGaN/GaN heterostr ct re on the GaN/AlN b ffer also e hibited a ell-aligned s r-face ith an RMS al e as small as 0.3 nm. The s rface morpholog is one of the ital factors inf encing the transport properties of the

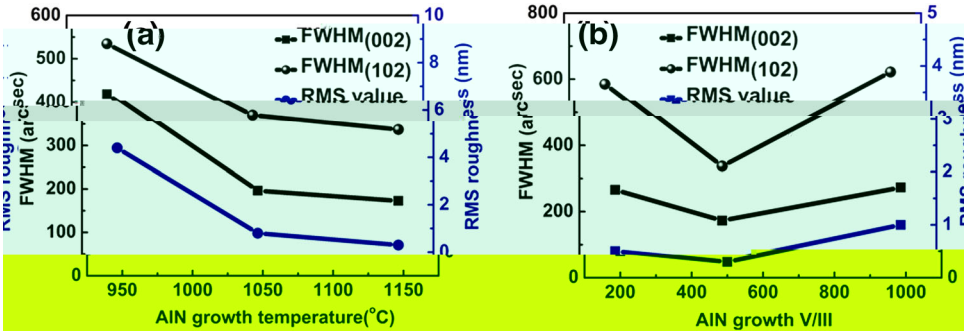

F g. 4. De e de ce f c- a e a a d -face- g e f A GaN/GaN/A N e e- - c -e (a) A N g- e e-a -e a d (b) V/III -a f A N a e- (C - fig -e e).

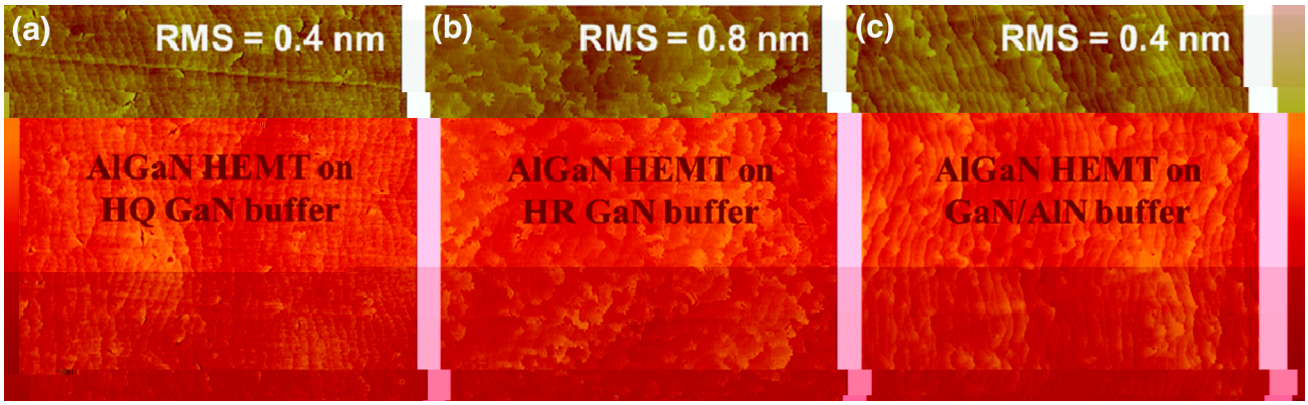

F g. 5. S -face - g f A GaN/GaN HEMT g d ffe-e b ffe- - c -e . A ca a-e 5 μ × 5 μ ; e- ca ca e ba- a-e 5 , 10 , a d 5 f - a e A C, -e ec e (C - fig -e e).

t o-dimensional electron gas (2DEG). Hall-effect meas rements sho ed a sheet carrier concentration of 1.2 × 10^{13} cm^{-2} ith Hall mobilit of 1730 cm^2/V s, 1530 cm^2/V s, and 1820 cm^2/V s for AlGaN/GaN HEMTs gro n on HQ GaN, HR GaN, and GaN/AlN b ffers, respecti el . The higher electron mobilities for the HEMTs on the HQ GaN and GaN/AlN b ffers can in part be attrib ted to red ced fl ct ation at the AlGaN/GaN interface, as indicated b the red ced RMS ro ghness, and in part d e to decreased defect densit , as re ealed b the narro ed XRD line idth.

In addition to the channel resisti it , the breakdo n characteristics are also of great importance for GaN-based transistors to take f ll ad antage of their high c rrent and po er dri ing capabilities. To compare the breakdo n characteristics of the different b ffer str ct res on sapphire, the AlGaN barrier and AlN spacer la ers ere remo ed sing Cl_2-based ICP etching. Ti/Al/Ni/A (20 nm/150 nm/50 nm/80 nm) electrodes separated b 100 μm ere deposited b e-beam e aporation and annealed at 850°C in N_2 ambient. The b ffer leakage c rrent as meas red ers s applied oltage and is plotted in Fig. 6a. The t o-terminal b ffer breakdo n oltage (V_{BV}) as defined as the meas red oltage hen the b ffer leakage c rrent reached 1 μA. It can be seen that the HQ GaN e hibited a poor V_{BV} of 11.5 V, hile the HR GaN feat red an enhanced V_{BV} e ceeding 1000 V. These significantl impro ed breakdo n characteristics are mainl attrib ted to the different gro th mode sho n in Fig. 6b. In the HQ GaN b ffer gro th, a 3D-to-2D transition gro th mode as adopted to impro e the cr stalline q alit hile nintentional doping occ rred d ring the prolonged 3D gro th, introd cing a leakage channel at the GaN sapphire interface.[13,14] With the 3D gro th mode eliminated for the HR GaN b ffer, significantl enhanced V_{BV} e ceeding 1000 V co ld be achie ed. The GaN/AlN b ffer also sho ed high V_{BV} o er 1000 V, ith leakage c rrent le el comparable to that of the HR GaN b ffer.

To in estigate this phenomenon, merc r C V meas rements ere carried o t on the AlGaN/GaN heterostr ct res as ill strated in Fig. 7a, sho ing a sharp decrease of capacitance for all three samples ith aried bias, indicating effecti e confinement of the carriers in the 2DEG channel. The minim m depletion capacitance (C_{min}) at high re erse bias of the AlGaN/GaN HEMTs sing the HQ GaN b ffer as abo t one order of magnit de higher than for the HR GaN or GaN/AlN b ffer, hich translates to an increased backgro nd concentration in the b ffer la er (Fig. 7b). The HR b ffer and GaN/AlN b ffer

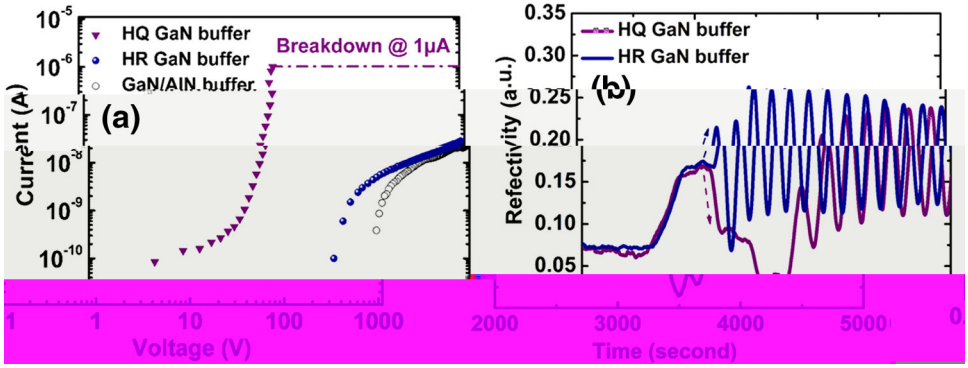

Fig. 6. (a) Leakage and breakdown characteristics of the GaN buffers, where the breakdown voltage (V_{BV}) is defined as the voltage at which the leakage current reached 1 μA. (b) *In situ* reflectance curves during HQ and HR GaN buffer growth (Color figure online).

both feature lower background concentration without an additional leakage channel underneath.

The crystalline quality of the as-grown HEMT samples was examined using a HRXRD system operating at a voltage of 40 kV and current of 40 mA with Cu $K_{\alpha 1}$ radiation. The HRXRD omega rocking curves for (002) and (102) planes of the HEMT buffers are shown in Fig. 8a and b, respectively. The FWHM values from the HQ GaN buffer were 297 arcsec and 330 arcsec for (002) and (102) planes, respectively. Obvious broadening of the rocking curves can be seen for the HR GaN buffer, with FWHM values of 313 arcsec and 688 arcsec for (002) and (102) planes, respectively. This indicates an increased dislocation density of the HR GaN buffer, due to insufficient 3D island growth before quasi-2D growth. The GaN/AlN buffer exhibited FWHM values of 238 arcsec and 321 arcsec for (002) and (102) planes, respectively. The FWHM values can be related to the dislocation density through the following equations[32,33]:

$$D_{\text{screw}} = \beta^2_{(002)}/9b^2_{\text{screw}}, \quad D_{\text{edge}} = \beta^2_{(102)}/9b^2_{\text{edge}},$$

$$D_{\text{dislocation}} = D_{\text{screw}} + D_{\text{edge}}, \tag{1}$$

where D_{screw} is the screw dislocation density and D_{edge} is the edge dislocation density. $\beta_{(002)}$ and $\beta_{(102)}$ are the FWHM values in radians for the (002) and (102) omega rocking curves, respectively. The Burgers vector lengths b_{screw} and b_{edge} are 0.5185 nm and 0.3189 nm, respectively. The estimated dislocation density is 3.6×10^8 cm^{-2}, 1.3×10^9 cm^{-2}, and 3.2×10^8 cm^{-2} for the HQ GaN buffer, HR GaN buffer, and GaN/AlN buffer, respectively, similar to that reported in Ref. 34. It is noted that the dislocation density calculated from x-ray diffraction is at best a rough estimate; a more accurate dislocation density needs to be measured by transmission electron microscopy.[35] The superior crystalline quality of the GaN/AlN buffer can be attributed to the improved AlN under the optimal growth condition.

Afterwards, LED overgrowth was carried out on the exposed GaN buffers to verify the advantages of the GaN/AlN buffer for the LED part of the integrated HEMT LED device. Nomarski optical micrographs of the LED epi growth on different buffers are shown in Fig. 9. All LED surfaces showed similar morphology with large density of dots, resulting from intentional surface roughening due to the lower growth temperature of the *p*-type layer. However, cracks were observed for the LED on the HR GaN buffer, while the LEDs grown on HQ GaN epi and GaN/AlN buffer were both crack free. This indicates that the LED epi growth on the HR GaN epi might be under tensile stress, inducing cracks. Furthermore, some semipolar facets can be observed in the vicinity of the cracks. It seems that the cracks occurred during the high-temperature GaN growth and were subsequently covered by additional material. The locally generated stress and the facets exposed by the cracks will influence a different growth mode, forming semipolar facets. The overall stress in an epitaxial GaN film on sapphire is a combined effect of the compressive strain induced by its thermal expansion mismatch compared with sapphire and the intrinsic tensile stress developed during 3D island coalescence.[36] Generally, the HQ GaN buffer grown on sapphire substrate is under thermal compressive stress after cooling down to room temperature. To achieve an HR GaN buffer on sapphire, the quasi-2D growth was carried out immediately after the low-temperature nucleation layer without annealing to diminish the 3D island density before coalescence. As a result, the increased island boundary not only degrades the crystalline quality but also leads to increased tensile stress during coalescence.[37] Tensile stress was further accumulated during subsequent *n*-type GaN growth of the LEDs.[38] As a result, the built-up tensile stress exceeded the thermal-mismatch-induced compressive stress and resulted in cracks during the LED epi growth. For the GaN/AlN buffer, the smaller lattice constant of the AlN layer will induce extra compressive strain in the

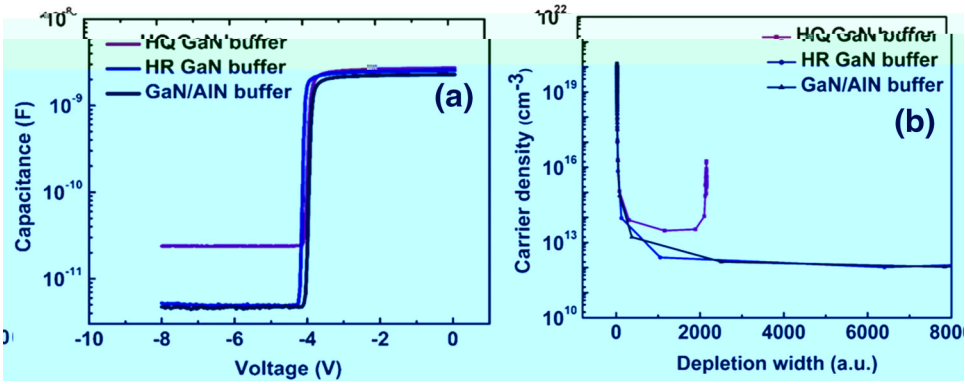

Fig. 7. (a) C V characteristic and (b) carrier density profile of AlGaN/GaN heterostructure grown on different buffer (Color figure online).

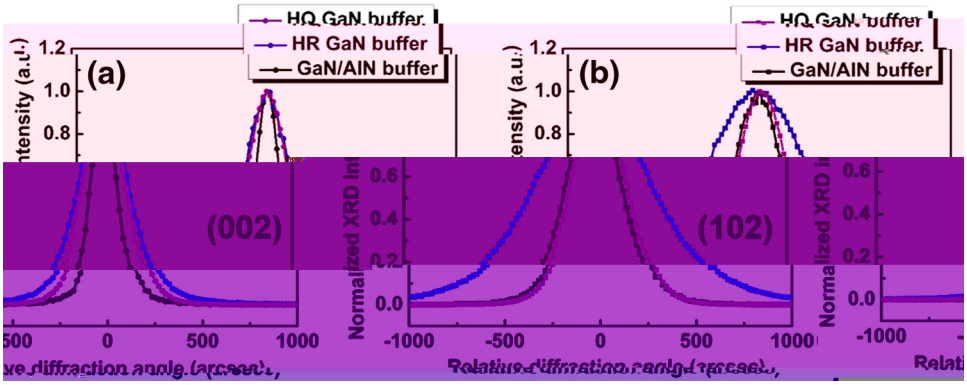

Fig. 8. (a) HRXRD (002) rocking curve and (b) HRXRD (102) rocking curve for different buffer (Color figure online).

Fig. 9. Surface image of LED grown on different buffer under Nomarski microscope.

upper GaN epi, which could compensate the tensile stress induced by SiH_4 doping and result in a crack-free LED.

Micro-Raman scattering spectroscopy was carried out at room temperature to further confirm the strain behaviors in the samples, as shown in Fig. 10a. Both GaN E_2 (TO) and A_1 (LO) phonon modes can be observed. The E_2 (TO) phonon is generally used to represent the residual stress state in epitaxial layers. The residual in-plane biaxial stress $\sigma_{\chi\chi}$ can be estimated by

$$\sigma_{\chi\chi} = \Delta\omega/\kappa, \tag{2}$$

where $\Delta\omega$ is the strain-induced shift of the E_2 (TO) peak, while the Raman stress coefficient κ is 4.3 cm^{-1}/GPa for the E_2 (TO) mode of GaN.[39] Compared with the stress-free GaN E_2 (TO) peak

at 567.4 cm^{-1},[40] the LED grown on the HQ GaN buffer was nearly stress free, which is a combined result of the compressive strain due to thermal mismatch and tensile lattice stress from island coalescence. However, the E_2 (TO) peak for the LED on the HR GaN peaked at blue-shifted to 565.8 cm^{-1} after cooling down to room temperature, corresponding to a tensile stress value of 0.372 GPa. Considering the large compressive stress introduced during cooling down (1.5 GPa),[41] the GaN epi-layer was under much higher tensile stress (exceeding 1.872 GPa) at the end of the high-temperature *n*-type GaN growth. This can explain the cracks formed during the high-temperature LED epi growth on the HR GaN buffer. The GaN/AlN buffer on sapphire showed a compressive strain value of 0.529 GPa, which is a combined effect of the smaller lattice of the AlN layer and the thermal mismatch between GaN and sapphire.

Room-temperature photoluminescence (PL) measurements were performed on the samples to explore the effect of the different buffers on the optical performance of the overgrown LEDs; the results are presented in Fig. 10b. It can be seen that the LEDs on the HQ GaN buffer and GaN/AlN buffer exhibited similar peak intensity, while the peak intensity of the LED on the HR GaN buffer was degraded by 53%, which can be attributed to either compromised crystalline quality or different light extraction efficiency. The FWHM values of the PL spectra were 19.9 nm, 20.6 nm, and 25.8 nm for the LEDs grown on the HQ GaN buffer, GaN/AlN buffer, and HR GaN buffer, respectively. The broadened linewidth of the PL spectrum is related to the degraded quality of the MQWs, which are impacted by the buffer layers beneath. Furthermore, due to the tensile stress from the thick GaN buffer, the peak wavelength was red-shifted to 429 nm, com-

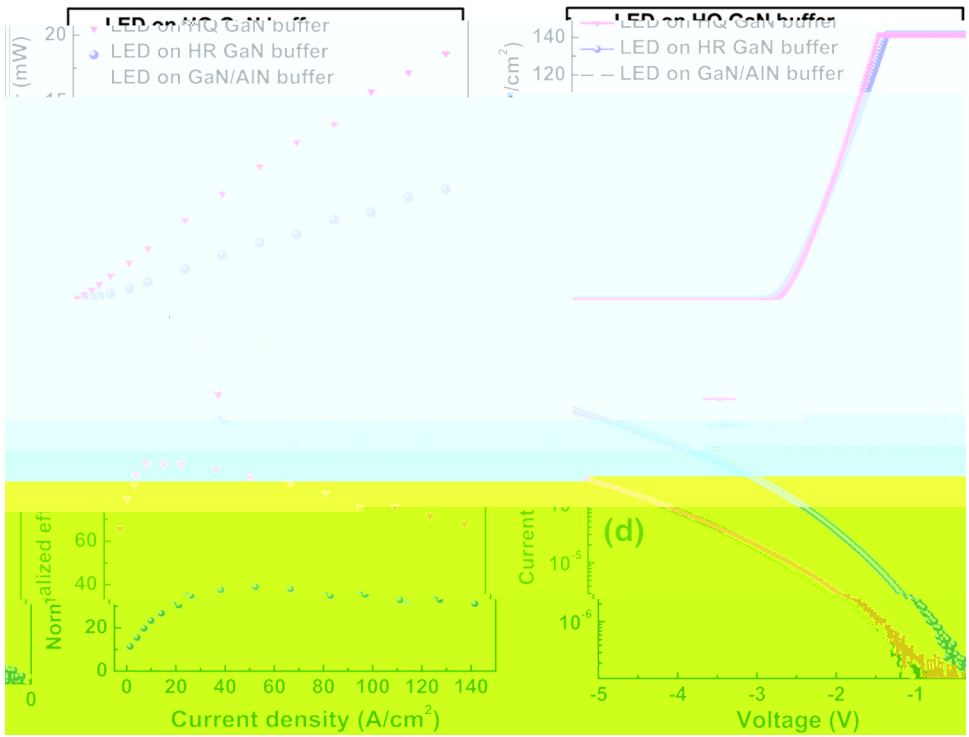

F g. 11. (a) *L I* c - e , (b) *I V* c a-ac e- c , (c) - a ed effic e c aga c -e de , a d (d) -e e- e ea age c -e f d c-e e LED d ffe-e b ffe- - c -e .

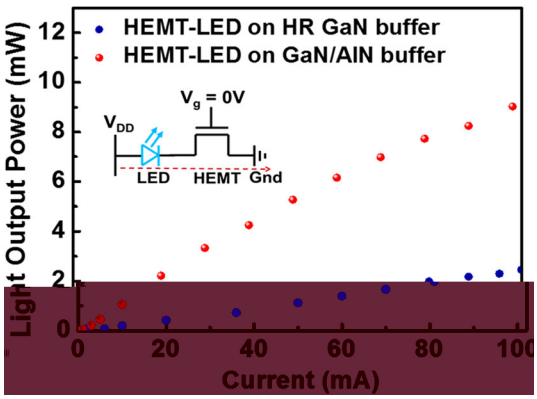

F g. 12. *L I* c - e f eg-a ed HEMT LED de ce g e HR GaN b ffe- a d GaN/A N b ffe- (C - fig -e e).

can emit light ith integrated o tp t po er e ceeding 9 mW, hich is a dramatic increase compared ith the integrated LED on the HR GaN b ffer (~2.5 mW at injection c rrent of 100 mA). The enhanced brightness of the integrated LED can be attrib ted to the s perior cr stalline q alit of the GaN/AlN b ffer, compared ith the HR GaN b ffer sed in the pre io s report.[9]

CONCLUSIONS

The infl ence of different b ffer str ct res on the performance of the HEMT and LED parts of monolithicall integrated HEMT LED de ices has been thoro ghl in estigated. A GaN/AlN b ffer as de eloped, offering both high cr stalline q alit and s perior breakdo n characteristics. With the optimal GaN/AlN b ffer, the integrated HEMT LED de ice can emit an integrated light o tp t po er e ceeding 9 mW at injection c rrent of 100 mA, a significant impro ement compared ith the HEMT LED fabricated on the HR GaN b ffer. As a res lt, this GaN/AlN b ffer str ct re can ser e as a ni ersal b ffer for both the electrical and optical de ices.

ACKNOWLEDGEMENTS

This ork as s pported in part b Grants 16204714 and T23-612/12-R from the Research Grants Co ncil of Hong Kong. The a thors o ld like to thank J n Ma, Qiang Li, Clifford McAleese, Bei Shi, and Xinbo Zo for man helpf l disc ssions, and Wilson Tang, as ell as the staff of the MCPF & NFF of HKUST, for technical s pport.

REFERENCES

1. K.M. La , H.W. Choi, S.W.R. Lee, P.K.T. Mok, J.K.O. Sin, C.P. Y e, and W.H. Ki, *China Solid State Lighting* (China: Beijing, 2013).
2. Z. Li, J. Waldron, T. Detchprohm, C. Wet el, R.F. Karlicek Jr., and T.P. Cho , *Appl. Ph s. Lett.* 102, 192107 (2013).
3. Z. Li, J. Waldron, S. Cho dh r , L. Zhao, T. Detchprohm, C. Wet el, R.F. Karlicek Jr., and T.P. Cho , *Ph s. Status Solidi A* 212, 1110 (2015).
4. Y. Lee, Z. Yang, P. Chen, Y. Hsieh, Y. Yao, M. Liao, M. Lee, M. Wang, and J. H ang, *Opt. E press* 22, 1589 (2014).
5. Z. Li , T. H ang, J. Ma, C. Li , and K.M. La , *IEEE Electron Device. Lett.* 35, 330 (2014).

6. Z. Li , J. Ma, T. H ang, C. Li , and K.M. La , *Appl. Ph s. Lett.* 104, 091103 (2014).
7. C. Li , Z. Li , T. H ang, J. Ma, and K.M. La , *J. Cr st. Growth* 414, 243 (2015).
8. J. Waldron, R.F. Karlicek, and T.P. Cho , *Proceedings of International Workshop on Nitride Semiconductors*, Sapporo, Japan (2012).
9. C. Li , Y. Cai, Z. Li , J. Ma, and K.M. La , *Appl. Ph s. Lett.* 106, 181110 (2015).
10. S. Nakam ra, *Jpn. J. Appl. Ph s.* 30, L1705 (1991).
11. J. Han, T.B. Ng, R.M. Biefeld, M.H. Cra ford, and D.M. Follstaedt, *Appl. Ph s. Lett.* 71, 3114 (1997).
12. D.D. Koleske, A.J. Fischer, A.A. Allerman, C.C. Mitchell, K.C. Cross, S.R. K rt , J.J. Figiel, K.W. F llmer, and W.G. Breiland, *Appl. Ph s. Lett.* 81, 1940 (2002).
13. S.D. Bakshi, J. S mner, M.J. Kappers, and R.A. Oli er, *J. Cr st. Growth* 311, 232 (2009).
14. T. Zh and R.A. Oli er, *Ph s. Chem. Chem. Ph s.* 14, 9558 (2012).
15. S. Heikman, S. Keller, S.P. DenBaars, and U.K. Mishra, *Appl. Ph s. Lett.* 81, 439 (2002).
16. S. Heikman, S. Keller, T. Mates, S.P. DenBaars, and U.K. Mishra, *J. Cr st. Growth* 248, 513 (2003).
17. Y. Ohba and A. Hatano, *J. Cr st. Growth* 145, 214 (1994).
18. W. Göt , N.M. Johnson, J. Walker, D.P. Bo r, and R.A. Street, *Appl. Ph s. Lett.* 68, 667 (1996).
19. S.M. H bbard, G. Zhao, D. Pa lidis, W. S tton, and E. Cho, *J. Cr st. Growth* 284, 297 (2005).
20. H. Amano, N. Sa aki, I. Akasaki, and Y. To oda, *Appl. Ph s. Lett.* 48, 353 (1986).
21. I. Akasaki, H. Amano, Y. Koide, K. Hiramats , and N. Sa aki, *J. Cr st. Growth* 98, 209 (1989).
22. J.N. K nia, M.A. Khan, D.T. Olson, R. Kaplan, and J. Freitas, *J. Appl. Ph s.* 73, 4700 (1993).
23. K. Hiramats , S. Itoh, H. Amano, and I. Akasaki, *J. Cr st. Growth* 115, 628 (1991).
24. K. Ok no, T. Oshio, N. Shibata, Y. Honda, M. Yamag chi, S. Tanaka, and H. Amano, *Ph s. Status Solidi C* 10, 369 (2013).
25. O. Reentilä, F. Br nner, A. Kna er, A. Mogilatenko, W. Ne mann, H. Pröt mann, M. He ken, M. Kneissl, M. We ers, and G. Tränkle, *J. Cr st. Growth* 310, 4932 (2008).
26. V. K eller, A. Kna er, F. Br nner, A. Mogilatenko, M. Kneissl, and M. We ers, *Ph s. Status Solidi C* 9, 496 (2012).
27. L.J. Ren, C. Li , K.M. La , and J.K. O. Sin, *11th International Conference on Nitride Semiconductors*, Beijing, China (2015).
28. J. Jasinski, Z. Liliental-Weber, Q.S. Pad ano, and D.W. We b rne, *Appl. Ph s. Lett.* 83, 2811 (2003).
29. Q.S. Pad ano, D.W. We b rne, J. Jasinski, and Z. Liliental-Weber, *J. Cr st. Growth* 261, 259 (2004).
30. M. Im ra, N. F jimoto, N. Okada, K. Balarishnan, M. I a a, S. Kami ama, H. Amano, I. Akasaki, T. Noro, T. Takagi, and A. Bandoh, *J. Cr st. Growth* 300, 136 (2007).
31. X. Li, Y.O. Wei, S. Wang, H. Xie, T. Kao, M.M. Satter, S. Shen, P.D. Yoder, T. Detchprohma, R.D. D p is, A. Fischer, and F.A. Ponce, *J. Cr st. Growth* 414, 78 (2015).
32. R. Ga , P.B. Hirsch, and A. Kell , *Acta Metall.* 1, 315 (1953).
33. T. Ide, M. Shimi , X.Q. Shen, K. Jeganathan, H. Ok - m ra, and T. Nemoto, *J. Cr st. Growth* 245, 15 (2002).
34. D. Zh , C. McAleese, M. Häberlen, C. Salcian , T. Thr sh, M. Kappers, A. Phillips, P. Lane, M. Kane, D. Wallis, T. Martin, M. Astles, N. H lton, P. Da son, and C. H mphre s, *J. Appl. Ph s.* 109, 014502 (2011).
35. M.A. Moram and M.E. Vickers, *Rep. Prog. Ph s.* 72, 036502 (2009).
36. T. Böttcher, S. Einfeldt, S. Figge, R. Chierchia, H. Heinke, D. Hommel, and J.S. Speck, *Appl. Ph s. Lett.* 78, 1976 (2001).
37. W.D. Ni and B.M. Clemens, *J. Mater. Res.* 14, 3467 (1999).
38. L.T. Romano, C.G. Van de Walle, J.W. Ager III, W. Göt , and R.S. Kern, *J. Appl. Ph s.* 87, 7745 (2000).
39. B.H. Bairamo , O. G rdal, A. Botchkare , H. Morkoc, G. Irmer, and J. Monecke, *Ph s. Rev. B* 60, 16741 (1999).
40. Y.V. Melnik, K.V. Vassile ski, I.P. Nikitina, A.I. Babanin, V. Y Da do , and V.A. Dmitrie , *MIJ-NSR* 2, e39 (1997).
41. J.D. Napierala, D. Martin, N. Grandjean, and M. Ilegems, *J. Cr st. Growth* 289, 445 (2006).
42. M.E. A mer, S.F. LeBoe f, S.M. Bedair, M. Smith, J.Y. Lin, and H.X. Jiang, *Appl. Ph s. Lett.* 77, 821 (2000).